

Pre-training and Fine-tuning Transformers for fMRI Prediction Tasks

Itzik Malkiel^{*,1} Gony Rosenman^{*,2} Lior Wolf¹ Talma Hendler²

¹School of Computer Science, Tel Aviv University

²Sagol School of Neuroscience, Tel Aviv University

Abstract

We present the TFF Transformer framework for the analysis of functional Magnetic Resonance Imaging (fMRI) data. TFF employs a transformer-based architecture and a two-phase training approach. First, self-supervised training is applied to a collection of fMRI scans, where the model is trained for the reconstruction of 3D volume data. Second, the pre-trained model is fine-tuned on specific tasks, utilizing ground truth labels. Our results show state-of-the-art performance on a variety of fMRI tasks, including age and gender prediction, as well as schizophrenia recognition.

Keywords: fMRI, Deep Learning, Self-supervision.

1. Introduction

Functional MRI (fMRI) is a non-invasive neuroimaging modality that captures spatio-temporal patterns of blood oxygenation in the behaving brain. The resulting Blood Oxygen Level Dependent (BOLD) signal and its relation to cognition are only partly understood, yet growing evidence suggests that the signal is highly informative regarding brain state and dynamics. Specifically, the BOLD signal was shown to be predictive with respect to the diagnosis and characterization of multiple neurological diseases and psychiatric conditions (Zhan and Yu, 2015; Woodward and Cascio, 2015; Xia et al., 2018).

Among medical imaging modalities, fMRI poses a unique challenge to machine learning due to the massive amount of signals acquired during a standard scan, which consists of a time series of 3D volumes, as well as the amount of noise that exists in the measurement device and the tradeoff between resolution and inherent noise caused by the patient’s motion, repeatability issues due to inter-patient and intra-patient variability, relatively small datasets due to the acquisition cost and privacy concerns, and often noisy target labels, which capture conditions that are often defined based on a group of symptoms (Kamitani and Tong, 2005).

Multiple advances in deep learning have been applied to fMRI classification, including convolutional-based models (Zou et al., 2017; Kawahara et al., 2017), recurrent neural networks (RNN) (Dakka et al., 2017), and graph neural networks (Li et al., 2020). Many of these techniques utilize well-known human brain atlases to parcellate the brain into regions. The parcellation process outputs a feature vector for each fMRI frame. The vectors are then used to train neural networks to make predictions, by extracting temporal information from this multivariate time-series data, constructing internal representations for brain connectivity, etc.

* Contributed equally.

In our work, we consider the entire, unparcellated, volume and apply end-to-end training using a hybrid network that includes a crucial transformer (Vaswani et al., 2017a) component. Transformers have emerged as a powerful model that employs multiple attention operations on sequential data. It has become the dominant model in time series forecasting (Li et al., 2019b; Wu et al., 2020), natural language understanding (Devlin et al., 2018; Yang et al., 2019; Liu et al., 2019), and, more recently, computer vision (Dosovitskiy et al., 2020; Li et al., 2019a; Lu et al., 2019).

In our work, we propose a network architecture for fMRI that is composed of a transformer model, which operates on feature vectors extracted from a 3D convolutional-based encoder. Our network, named TFF, extracts vectors from the raw 3D-volume brain fMRI samples, constructs the vectors as a unified sequence, and propagates them through a multi-layer transformer network. In our research, we fine-tune TFF on multiple datasets, such as the dataset of the Human Connectome Project (Van Essen et al., 2013) and the COBRE¹ and CNP² Schizophrenia datasets. We report state-of-the-art performance for various tasks, including age and gender prediction, as well as diagnosing Schizophrenia.

2. Related Work

Traditional approaches to fMRI data employ a pipeline that first applies a parcellation process to the raw fMRI signal (Arslan et al., 2018). A parcellation procedure aggregates spatially neighboring voxels into local clusters, which represent regions of interests (ROIs). The voxels associated with the same ROIs are averaged and concatenated into a vector, representing a single volumetric fMRI 3D data point. Applied to the entire 4D fMRI scans, the parcellation process retrieves multivariate time-series data, where each sample is a multi-dimensional vector associated with a single 3D fMRI frame.

Next, given the parcellated data, most techniques infer a functional connectivity (FC) matrix, which is a scalar function that scores the temporal relation between two different regions in the brain. A common FC measure is the Pearson correlation, also known as Static Functional Connectivity (van den Heuvel and Hulshoff Pol, 2010). The FC matrix representing the brain activity, which is also known as the “connectome”, has attracted significant interest in the field of neuroscience as a sensitive biomarker for diseases. Finally, supervised machine learning techniques are applied in order to obtain predictions at the level of the individual.

Inspired by the above pipeline, data-driven approaches were applied in order to obtain a more effective FC function and/or better representations for the parcellated data. In (Riaz et al., 2020), the authors propose a deep learning model for generating dynamic FC functions. Using 1D convolutions on parcellated time series, the authors compute a learned feature vector for each ROI. Next, all vector pairs are concatenated and scored by a learned multilayer perceptron (MLP), producing an effective pairwise similarity matrix. Finally, the resulting matrix is propagated through another MLP, applying end-to-end training via the classification objective.

In (Gadgil et al., 2020), the authors suggest applying Spatial-Temporal Graph Convolutional Networks (ST-GCN), a computer vision technique, for learning from graph-structured

¹http://fcon_1000.projects.nitrc.org/indi/retro/cobre.html

²<https://openneuro.org/datasets/ds000030/versions/00016>

time series data (Yu et al., 2017). The authors leveraged ST-GCN for age and gender prediction from parcellated fMRI data. In our work, we evaluate TFF on the same task and dataset reported in (Gadgil et al., 2020), and observe superior performance compared to previous reports.

Our 3D convolutional encoder and decoder network architecture build upon the network developed by Myronenko (2018b) for the purpose of brain tumor segmentation from 3D MRI data. Their architecture receives 3D MRI crops as its input, and utilizes a sequence of convolutional blocks with skip connections. The encoder output is fed into two decoder heads. The first is trained with supervision to predict segmentation. The second decoder head is trained using self-supervision to reconstruct the input volume data by employing a variational auto-encoder approach. In our work, we adopt the building blocks of the architecture, omit the decoder head that performs segmentation and modify the head that performs reconstruction by removing the variational auto-encoder mechanism. In order to support 4D fMRI data and enable the model to obtain and process temporal information, we add the transformer architecture between the encoder and the decoder.

3. Method

The TFF framework utilizes both 3D convolutional layers and transformer layers, and applies a pre-training and a subsequent fine-tuning approach, see Fig. 1. The model utilizes a convolution-based encoder \mathcal{E} , which operates separately on acquired 3D fMRI frames (each frame is a snapshot of the subject’s brain activity at time t), mapping each frame into a vector. Next, the model proceeds by aggregating vectors of consecutive frames into a unified sequence, and propagating the sequence through a transformer network \mathcal{T} .

During pre-training, the transformer output is propagated through a decoder \mathcal{D} that supports self-supervision through reconstructing the original input. During fine-tuning, \mathcal{D} is removed, and \mathcal{E} and \mathcal{T} are optimized directly for the given task, in an end-to-end manner.

3.1. Pre-Training

TFF pre-training employs a two-step training procedure. The first step trains the 3D-convolutional encoder-decoder networks for reconstruction (more details can be found in the architecture section). Given an fMRI scan, with n frames, $X := (x_1, \dots, x_n)$, where each x_i is a volumetric data point representing the acquired pulses and echoes in a given interval, $x_i \in R^{W \times H \times D}$ where W, H, D are the width, height, and depth of the acquired data, we first map each frame into two representations by applying two normalization techniques. The first technique applies a *global normalization*, utilizing standard z-score normalization over the entire scan. The second applies a *voxel normalization*, which separately z-score normalizes the values of each voxel over the time domain.

The global normalization, denoted by X^g , can be expressed as:

$$X^g := \frac{X - \mu}{\sigma} \quad (1)$$

where μ, σ are the mean and standard deviation of the entire 4D volume X . By focusing on the qpk dimension of a specific frame, the voxel normalization, denoted by X^v , can be

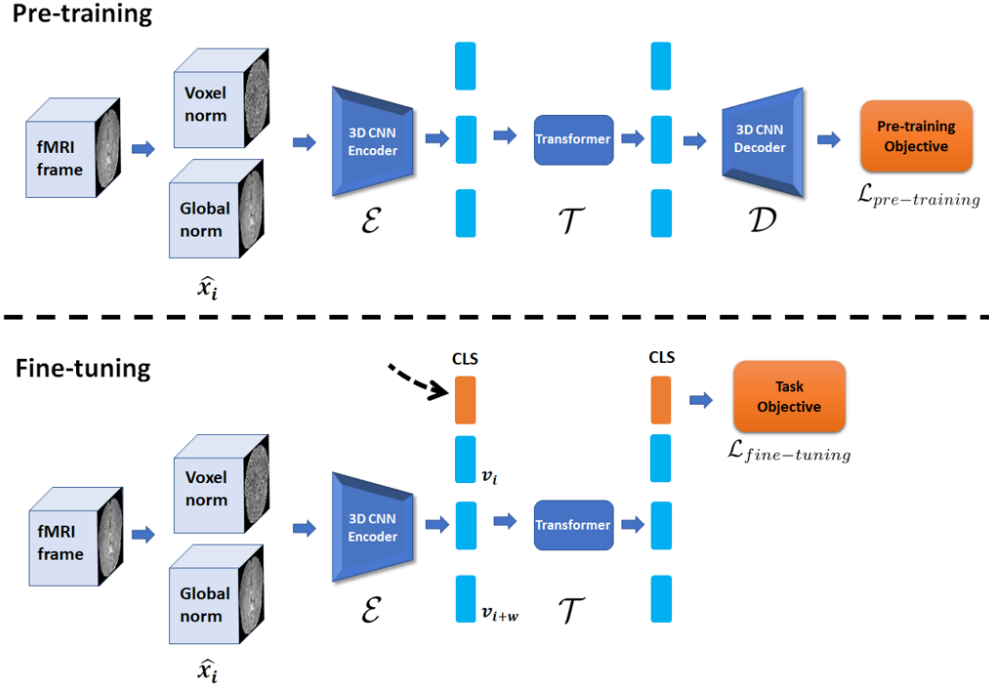


Figure 1: Illustration of the TFF architecture. During pre-training (top), a sequence of fMRI frames are normalized and propagated through the 3D CNN encoder network \mathcal{E} (shown is a single frame of a sequence of w frames). The encoder outputs a single vector for each input frame. The vectors are grouped into a unified sequence and propagated through the transformer network \mathcal{T} . The output sequence is decomposed, aggregated on the batch dimension, and propagated through the decoder \mathcal{D} , which reconstructs the input data. During fine-tuning (bottom), a sequence of fMRI frames are propagated separately through the pre-trained encoder network. The vectors are aggregated as a sequence and a special CLS token is concatenated to the beginning of the sequence. The entire sequence is then propagated through the transformer model, which utilizes the embedding of the CLS token for making predictions. During pre-training and fine-tuning, the model is trained in an end-to-end manner.

expressed as follows:

$$x_{i_{qpk}} = \frac{x_{i_{qpk}} - \mu_{qpk}}{\sigma_{qpk}} \quad (2)$$

where μ_{qpk}, σ_{qpk} are the mean and standard deviation of the voxel qpk , across all frames in X .

Voxel normalization emphasizes the relative activation of a specific voxel in a given interval, while suppressing the structural information, see Fig. 2). We denote the concatenation on the channel dimension of the two normalized representations of the entire scan as $\hat{X} := (\hat{x}_1, \dots, \hat{x}_n)$.

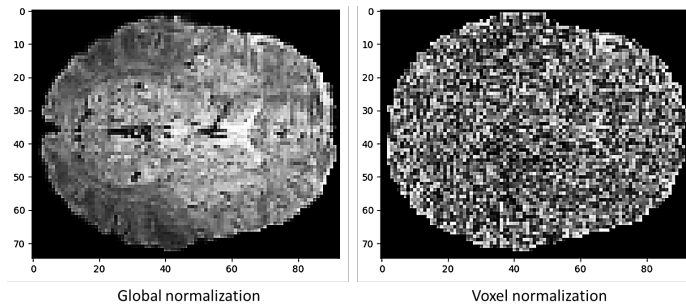


Figure 2: A representative 2D slice from an acquired 3D fMRI frame, applied through global normalization (left) and voxel normalization (right). Global normalization applies the same scaling and shifts to all voxels, yielding a volume that is visually similar to the original volume. Voxel normalization scales and shifts each voxel separately, by looking at its values across the entire scan. The resulting voxel-normalized data surpasses structural information and emphasizes voxels associated with values that are far from their mean value.

Next, given \hat{X} , we extract a sub-sequence of frames \hat{x}^w with length w and aggregate the frames on the batch dimension. The batches of the frames are then propagated through the encoder and the decoder, which outputs data of the same dimension as the input frames. The model is trained to optimize two pixel-wise losses and a perceptual loss, as described below in the section on pre-training loss term, to reconstruct the global normalized data.

The encoder-decoder architecture imposes a bottleneck with a size of d . This bottleneck entails that each x_i is represented by a single vector $v_i \in \mathcal{R}^d$. Notably, the convolution-based encoder and decoder networks operate on each frame *separately*, i.e., the convolutions are not applied on batches of frames, and therefore, at this stage, the model cannot extract temporal information.

After the first pre-training stage, we insert the transformer model \mathcal{T} between the two convolution-based encoder and decoder networks and proceed with the same pre-training procedure, using the same reconstruction loss. In this second stage, the transformer architecture enables the model to obtain and process information from the time domain, while training continues in order to optimize the same objective.

In TFF, we adopt a standard transformer architecture (Vaswani et al., 2017b). The model first aggregates the vectors provided by \mathcal{E} into a unified sequence and adds a special *CLS* token to the beginning of the sequence. The sequence can be denoted by $(CLS, v_i, \dots, v_{i+w})$, where w is a window hyperparameter dictating the length of input sequences. Next, the sequence is propagated through the \mathcal{T} and its output is propagated through the 3D CNN decoder \mathcal{D} . In both pre-training stages, we feed the model with the 2-norm data \hat{X} , while training it to only reconstruct globally normalized data.

The two-stage pre-training scheme, chosen over the alternative of a single pre-training phase that optimizes the entire model, stems from the empirical observation that a single training phase is unstable. Specifically, in our study, we observed the vanishing gradients

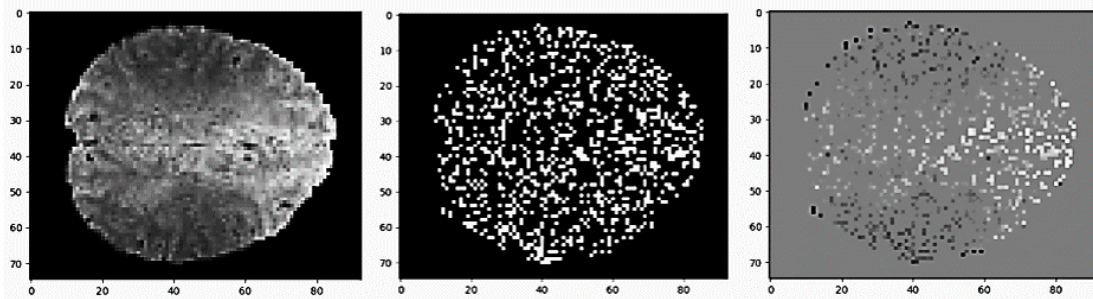


Figure 3: A representative sample of a slice (left) and its voxels that contribute to the intensity loss (right). The intensity loss emphasizes the voxels that vary the most in a given frame, by leveraging a “focused” L1 loss applied to those specific voxels. To calculate this loss, we infer a binary mask for each of the slices (middle).

phenomenon when pre-training a transformer on top of randomly initialized 3D convolution layers. Additional information can be found in the Experiments section.

3.2. The Pre-Training Losses

During pre-training, we employ two pixel-wise losses and a perceptual loss. The first loss, denoted by \mathcal{L}_1 , is a standard L1 loss that is applied between the decoder output and the globally normalized frames X^g .

The second loss is an intensity loss, denoted as \mathcal{L}_1^b . This loss is based on an L1 applied to a subset of the voxels associated with local intensity values, which are more likely to represent a relevant BOLD signal. More specifically, given a full scan, (x_1, \dots, x_n) , we infer the voxel-normalization X^v . Then, for each voxel-normalized frame $x_i^v \in X^v$, we set:

$$x_{ipqk}^v = \begin{cases} 0 & |\hat{x}_{ipqk}^v| < b \\ \hat{x}_{ipqk}^v & \text{otherwise} \end{cases} \quad (3)$$

where b is a threshold value configured as the 80% quantile of the absolute of the voxel-normalized values, inside the anatomy and across the sub-sequence. The motivation behind the elimination of the voxels associated with the 80% of the values that are closer to 0 is that these values are typical across many frames, and are therefore unlikely to represent a distinctive signal. An illustration of the voxels that contribute to the intensity loss is depicted in Fig. 3.

The third loss is a standard perceptual loss, denoted by \mathcal{L}_p . Here we use a pre-trained VGG network (Simonyan and Zisserman, 2014), for which we minimize the L1 distance between the feature maps of the second and third layers extracted from the reconstructed data and input frames. Note that, unlike many perceptual loss terms that focus on the high-level features, we focus on low-level features, since our work is in a domain far removed from ImageNet, making the high-level features less relevant for this data.

Therefore, TFF utilizes only the first and second VGG layers, which are known to be more sensitive to edges. To adapt the perceptual loss for 3D data, we construct two batches.

The first is the concatenation of the slices of the input data, and the second holds the slices of the reconstructed data. Each batch is propagated separately through the VGG model. The perceptual loss is calculated over the pairs of corresponding slices from each batch and mean-pooled across the different slice-pairs.

Finally, the total pre-training objective is:

$$\mathcal{L}_{pre-training} = \mathcal{L}_1 + \mathcal{L}_1^b + \mathcal{L}_p \quad (4)$$

3.3. Model Architecture

Our model is composed of a 3D convolution-based encoder, followed by a transformer network. During pre-training, an additional 3D convolutional decoder is used to reconstruct the input data from the transformer output.

For the convolution-based encoder and decoder models, we build on the architecture introduced in (Myronenko, 2018a). Specifically, the encoder is composed of a sequence of four blocks, each block comprising a 3D convolutional layer, followed by a dropout layer (Srivastava et al., 2014), group normalization layer (Wu and He, 2018), ReLU, convolutional layer, groupNorm layer, and another ReLU. Finally, a down-sample layer is applied by utilizing a 3D convolutional layer with a stride of two. The output of the last block is then flattened, forming a 1D feature vector of size 2640. Notably, each of the elements in the flattened vector corresponds to a receptive field of 8X8X8 in the original volumetric input.

The transformer architecture is composed of a two-layer multi-head transformer (Vaswani et al., 2017a). This network also utilizes a standard positional encoding layer, in which its output is summed with the intermediate vectors (similar to standard language models such as (Devlin et al., 2018)).

The decoder architecture applies the same number of convolutional blocks, with similar layers, except for the final down-sampling layer which is replaced by an up-sampling layer. Our code for the training, network architecture, and results is attached as supplementary material³.

3.4. Fine-Tuning

During fine-tuning, we load the pre-trained model, without the decoder layers (i.e. we load the \mathcal{E} and \mathcal{T} networks), and optimize the model with supervision to perform the specific task at hand. In our study, we perform both classification and regression tasks. To fine-tune the model on such tasks, we add a standard classification (regression) head on top of the embedding of the CLS token and optimize a standard classification (regression) loss.

The fine-tuning objective can be expressed as:

$$\mathcal{L}_{fine-tuning} = -\sum_{i=1}^m \mathcal{L}_{cce}(y_i, \mathcal{C}(\mathcal{T}[\mathcal{E}(\hat{x}_i^w)]_0)) \quad (5)$$

where x_i^w is a sub-sequence of frames with length w associated with the label $y_i \in [1...c]$ (c is the number of classes), \mathcal{C} is the classification (or regression) head. m is the number of sub-sequences in the train set, and \mathcal{L}_{cce} is a softmax function followed by a standard categorical cross-entropy loss. For a binary classification task, we use the same loss by defining $c = 2$. For regression tasks we replace the cross-entropy with a standard MSE.

³<https://github.com/GonyRosenman/TFF>

3.5. Inference

Given a scan X , we infer \hat{X} , and extract all sub-sequences of length w and stride s . The TFF inference can be written as follows:

$$\text{TFF}_{\mathcal{I}} := \frac{\sum_{i=0}^m \mathcal{C} \left(\mathcal{T} \left[\mathcal{E} \left(\left(\hat{X} \right)_{si}^{si+w} \right) \right]_0 \right)}{m} \quad (6)$$

where m is the number of sub-sequences for the given stride s and 0 stands for the index of the CLS token.

4. Experiments

We evaluate our model on four tasks and three datasets and compare its performance to three baselines. While it is possible to pre-train our model on multiple datasets, this would hinder our ability to compare it directly with previous work. Therefore, in this study, we pre-train our models separately on each of the given datasets.

4.1. The Datasets

The Human Connectome Project (HCP) is a collection of publicly available functional MRI scans (Van Essen et al., 2013). The dataset contains 1095 scans of different subjects, 595 females and 500 males. The age of the subjects ranges between 22 and 36. Each scan includes 1200 fMRI frames, acquired while subjects were in a resting state. The scans were pre-processed by the HCP functional pipeline available from the Connectome DB website⁴. In TFF, the HCP data is applied without any additional pre-processing, beyond the pipeline used in the Connectome DB project. In our study, we focus on predicting age (regression task) and gender (binary classification) from fMRI scans. These tasks can help shed light on the relationship between brain activity, age, and gender, especially in the context of neuropsychiatric research. In our experiments, we split the data randomly into train, validation, and test sets, with respective sizes of 765, 110 and 220.

The Center for Biomedical Research Excellence (COBRE) is a dataset containing functional MRI data of 75 healthy control patients along with 72 schizophrenia patients diagnosed using the Structured Clinical Interview for DSM Disorders. The dataset was obtained from the Neuroimaging Informatics Tools and Resources Clearinghouse (NITRC) website and was published by the Center of Biomedical Research Excellence⁵. The COBRE Dataset excludes subjects who are pregnant, suspected to be pregnant, have neurological disorders, or have intellectual disabilities. Given the fMRI scans, the task we consider is to predict whether a subject is healthy or should be diagnosed with schizophrenia (binary classification). The data were split randomly into train, validation, and test sets, with respective sizes 102, 14, and 30.

⁴<https://db.humanconnectome.org/app/template/Login.vm>

⁵http://fcon_1000.projects.nitrc.org/indi/retro/cobre.html

Consortium for Neuropsychiatric Phenomics (CNP) is an fMRI dataset acquired as part of the UCLA Consortium for Neuropsychiatric Phenomics LA5c Study (Gorgolewski et al., 2017)⁶. All patients were assessed with the Structured Clinical Interview for the DSM (Fourth Edition). The dataset incorporates fMRI scans of 130 healthy controls subjects and 50 subjects diagnosed with schizophrenia. Here, too, the task we consider is the binary schizophrenia classification based on the acquired fMRI scans. The dataset was divided randomly into train, validation, and test sets, with sizes of 140, 20, and 20, respectively.

The exact train-validation-test splits, and more information about all datasets can be found in the supplementary appendix.

4.2. The Baselines

Spatial-Temporal Graph Convolutional Networks (ST-GCN) is a computer vision technique for learning from graph-structured time series data (Yu et al., 2017). It employs several spatio-temporal convolutional blocks alternating with spatial graph convolution layers. A very recent work proposed leveraging ST-GCN for age and gender prediction from fMRI scans (Gadgil et al., 2020). In the ST-GCN baseline, fMRI data is parcellated into multiple major Region Of Interests (ROI), and the average BOLD signal in each region is z-score normalized and fed into the network. Gadgil et al. (2020) then apply ST-GCN on the HCP dataset, reporting that the obtained accuracy is significantly higher than traditional CNN- and RNN-based methods.

Deep-fMRI is an end-to-end deep learning architecture for classifying pathologies in fMRI data (Riaz et al., 2020). It receives pre-processed parcellated fMRI signals as input and outputs a diagnosis. The model comprises a three-component architecture. The first component applies a convolution-based network to extract features from the input signals of the entire scan. This network outputs a 32-element vector for each brain region. The second component is a network that operates on all pairs of brain regions by concatenating the 32-dimensional vectors and propagating them through an MLP regression layer. Based on all brain region pairs, the network predicts a correlation matrix for each of the region-pairs. The last component is an MLP classification network, which makes predictions based on the estimated correlation matrix. The Deep-fMRI model is trained in an end-to-end manner, optimizing the standard classification loss. In (Riaz et al., 2020), the authors report that Deep-fMRI outperforms other alternatives such as correlation-based functional connectivity, clustering-based technique, as well as the FCNet model (Riaz et al., 2017), which is another convolution-based model.

$TFF_{\text{no-pre-training}}$ is the TFF model initialized from scratch and performed without the pre-training procedure. In other words, only the fine-tuning training for the task at hand is performed.

4.3. The Metrics

The following metrics are reported for the classification tasks: accuracy, balanced accuracy (BAC), and Area Under the Receiver Operating Characteristic curve (AUROC). For the

⁶<https://openneuro.org/datasets/ds000030/versions/00016>

Table 1: Gender prediction results on the HCP dataset.

Model	BAC	Acc.	AUC
TFF TFF _{no-pre-training}	93.18	92.06	95.34
ST-GCN	82.0	79.81	81.36
Deep-fMRI	66.91	65.45	78.0

Table 2: Age prediction results on the HCP dataset (regression task, lower is better).

Model	L1	L2	NMSE $\times 10$
TFF	2.73	10.93	0.14
TFF _{no-pre-training}	3.21	14.13	0.19
ST-GCN	3.16	13.53	0.18
Deep-fMRI	3.48	17.59	0.25

regression task, we report the L1, L2, and the Normalized Mean Square Error (NMSE) metrics. The NMSE metric is defined as:

$$NMSE(\hat{y}, y) = \frac{MSE(\hat{y}, y)}{MSE(y, 0)} = \frac{\|\hat{y} - y\|_2^2}{\|y\|_2^2} \quad (7)$$

where \hat{y}, y are the predicted and the ground truth values, respectively.

4.4. implementation details

TFF utilizes the AdamW (Loshchilov and Hutter, 2017) optimizer, with a weight decay of 0.01. The window size is set to $w = 20$, with a stride of $s = 10$. The encoder architecture imposes an intermediate feature vector of size $d = 2640$. In our experiments, all TFF pre-training and fine-tuning used a single GPU (either V100 or Titan X), and each single-step training procedure ran for less than 24 hours, with a standard early stopping strategy. In most cases, the cumulative time of the two-step pre-training is below 28 hours, and the fine-tuning converges within 5-18 hours (depending on the task).

4.5. Results

Tab. 1 presents the results of all models evaluated on the HCP dataset for the gender prediction task. The TFF model was pre-trained on the HCP dataset, according to our proposed training and objective. All models were fine-tuned with supervision, utilizing the gender labels available for each subject in the HCP dataset. As can be seen in the table, TFF outperforms the alternatives by a sizeable margin. Specifically, compared to the ST-GCN model, which was previously considered state-of-the-art for this task, our model yields an improvement of more than 10% in BAC. Interestingly, we observe that the TFF full method also outperforms the TFF_{no-pre-training} baseline with ~ 0.8 , ~ 2 and ~ 3.4 points of BAC, accuracy and AUC, respectively.

Table 2 depicts the performance of all models evaluated on the age prediction task from the HCP dataset. This task is formulated as a regression task, where the models are expected

Table 3: Schizophrenia classification results on the COBRE dataset (a classification task)

Model	Accuracy	AUC	BAC
TFF	70.0	68.3	69.2
TFF _{no-pre-training}	43.3	44.2	44.2
ST-GCN	57.2	64.3	58.6
Deep-fMRI	68.3	62.0	65.6

Table 4: Schizophrenia classification results on the CNP dataset (classification task)

Model	Accuracy	AUC	BAC
TFF	88.2	90.0	87.9
TFF _{no-pre-training}	58.8	52.9	50.0
ST-GCN	82.3	87.1	82.8
Deep-fMRI	76.5	84.3	77.9

to predict the exact age of each subject. Each of the models in this evaluation applies a standard regression head and optimizes an L1 loss w.r.t the ground truth age labels. As can be seen in the table, TFF shows a clear advantage over the other techniques. Compared to ST-GCN, the second best model in this evaluation, TFF yields an absolute improvement of ~ 0.4 , ~ 2.6 on L1 and L2 respectively, and a relative improvement of 23% in NMSE. Interestingly, the gap in performance is even larger in comparison to the TFF_{no-pre-training} baseline, for which TFF improves in absolute scores of ~ 0.4 , ~ 3.2 for L1 and L2, and a relative improvement of $\sim 26\%$ in NMSE. This can be attributed to the importance of the pre-training procedure, which allows TFF to learn an effective representation for 4D fMRI data prior to the fine-tuning procedure.

We further evaluate our models on two datasets for pathological classification. Tab. 3 presents the results for schizophrenia classification on the COBRE dataset. As can be seen in the table, TFF outperforms the alternatives by a sizeable margin. Looking at the AUC score, TFF outperforms ST-GCN and DeepfMRI by 4 and 8.3 points, respectively. Interestingly, by neglecting the pre-training procedure, the TFF_{no-pre-training} fails to converge on the task. This can be attributed to (1) the relatively smaller number of samples, which hinders the ability of the TFF_{no-pre-training} model to generalize correctly in the case of unseen samples, and (2) to the importance of the pre-training procedure for extracting valuable features in advance, which is crucial to the convergence of the fine-tuning procedure.

Tab. 4 presents the evaluation results of the various models on the CNP dataset. As can be seen, the TFF model greatly outperforms the alternatives. Specifically, TFF retrieves a BCA score of 87.9, an improvement of more than 5.1 and 10 absolute points, respectively, over the ST-GCN and Deep-fMRI baselines. Looking at the TFF_{no-pre-training} baseline, we observe that the model suffers from poor performance.

By comparing the convergence of TFF and TFF_{no-pre-training} during the shared fine-tuning stage, which is presented in Fig. 4, we observe that the TFF_{no-pre-training} model struggles to converge, while the proposed model produces better results across the entire course of

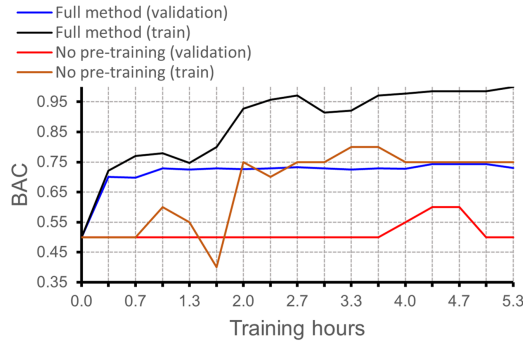


Figure 4: BAC vs train time on the validation and train sets of CNP dataset for the TFF and TFF_{no-pre-training} models.

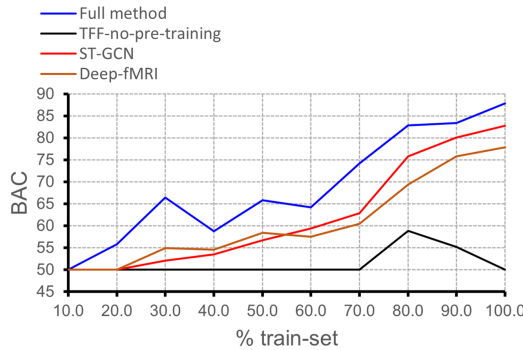


Figure 5: Balanced accuracy for a fraction of the train set used.

training. Once again, we attribute the enhanced performance of TFF to the effectiveness of the pre-training procedure.

4.6. Variable Train Size

We vary the amount of data available for training and evaluate the performance of each model for schizophrenia classification on the CNP dataset. The results, as shown in Fig. 5, indicate that the performance of all four methods drops significantly when the amount of training data is reduced. It is also evident that for all training set sizes the full TFF method is better than the baselines.

4.7. Ablation Study

Table 5 presents an ablation study for TFF on the age prediction and gender prediction tasks. The following variants are considered: (i) TFF without intensity loss. (ii) TFF without L1 loss. (iii) no perceptual loss. (iv) training TFF solely on the global normalization data (i.e. neglecting the voxel-normalization input). (v) TFF with a one-step pre-training, which trains all three networks \mathcal{E} , \mathcal{T} , \mathcal{D} in one phase. Different from the full method, this model optimizes the transformer weights on top of a randomly initialized encoder \mathcal{E} .

Table 5: Ablation study, see text for variants (i)–(v).

	Age pred.			Gender pred.		
	L1	L2	NMSE	Acc.	BAC	AUC
(i) no intensity loss	2.96	11.71	0.16	93.77	92.95	96.06
(ii) no L1 loss	3.12	13.07	0.18	89.66	87.43	91.25
(iii) no perceptual loss	3.02	12.11	0.17	93.47	93.02	96.86
(iv) no 2-norm	3.09	12.65	0.17	93.07	92.96	93.37
(v) one-step pre-train	3.21	14.33	0.19	89.97	91.02	90.38
Full method	2.73	10.93	0.14	94.09	93.92	98.77

The results, shown in Tab. reftab:ablation, indicate that it is highly beneficial to employ all three losses during the pre-training procedure, that voxel-normalization is crucial for model convergence, and that two-step pre-training is a better alternative to a single step.

5. Conclusions

TFF is a novel framework for the analysis of fMRI data. It considers the entire 4D fMRI volume data and applies end-to-end training using a transformer-based architecture. The TFF training consists of two phases, a self-supervised pre-training procedure and the subsequent fine-tuning, which optimizes the model for a specific task. Importantly, the pre-training procedure was found to be crucial for improved accuracy. Our experiments demonstrate state-of-the-art performance on a variety of fMRI tasks, including age and gender prediction, as well as schizophrenia recognition. One of the properties of TFF, which was not considered in this work, is that it can be pre-trained on a large amount of unlabeled data, and fine-tuned on relatively smaller-sized datasets, which are common in the field of medical imaging.

References

- S. Arslan, S. I. Ktena, A. Makropoulos, E. C. Robinson, D. Rueckert, and S. Parisot. Human brain mapping: A systematic comparison of parcellation methods for the human cerebral cortex. *Neuroimage*, 170:5–30, 04 2018.
- Jumana Dakka, Pouya Bashivan, Mina Gheiratmand, Irina Rish, Shantenu Jha, and Russell Greiner. Learning neural markers of schizophrenia disorder using recurrent neural networks. *arXiv preprint arXiv:1712.00512*, 2017.
- Jacob Devlin, Ming-Wei Chang, Kenton Lee, and Kristina Toutanova. Bert: Pre-training of deep bidirectional transformers for language understanding. *arXiv preprint arXiv:1810.04805*, 2018.
- Alexey Dosovitskiy, Lucas Beyer, Alexander Kolesnikov, Dirk Weissenborn, Xiaohua Zhai, Thomas Unterthiner, Mostafa Dehghani, Matthias Minderer, Georg Heigold, Sylvain Gelly, Jakob Uszkoreit, and Neil Houlsby. An image is worth 16x16 words: Transformers for

- image recognition at scale. *CoRR*, abs/2010.11929, 2020. URL <https://arxiv.org/abs/2010.11929>.
- Soham Gadgil, Qingyu Zhao, Adolf Pfefferbaum, Edith V Sullivan, Ehsan Adeli, and Kilian M Pohl. Spatio-temporal graph convolution for resting-state fmri analysis. In *International Conference on Medical Image Computing and Computer-Assisted Intervention*, pages 528–538. Springer, 2020.
- Krzysztof J Gorgolewski, Joke Durnez, and Russell A Poldrack. Preprocessed consortium for neuropsychiatric phenomics dataset. *F1000Research*, 6, 2017.
- Yukiyasu Kamitani and Frank Tong. Decoding the visual and subjective contents of the human brain. *Nature neuroscience*, 8(5):679–685, 2005.
- Jeremy Kawahara, Colin J Brown, Steven P Miller, Brian G Booth, Vann Chau, Ruth E Grunau, Jill G Zwicker, and Ghassan Hamarneh. Brainnetcnn: Convolutional neural networks for brain networks; towards predicting neurodevelopment. *NeuroImage*, 146: 1038–1049, 2017.
- Liunian Harold Li, Mark Yatskar, Da Yin, Cho-Jui Hsieh, and Kai-Wei Chang. Visualbert: A simple and performant baseline for vision and language, 2019a.
- Shiyang Li, Xiaoyong Jin, Yao Xuan, Xiyu Zhou, Wenhui Chen, Yu-Xiang Wang, and Xifeng Yan. Enhancing the locality and breaking the memory bottleneck of transformer on time series forecasting. In H. Wallach, H. Larochelle, A. Beygelzimer, F. d'Alché-Buc, E. Fox, and R. Garnett, editors, *Advances in Neural Information Processing Systems*, volume 32. Curran Associates, Inc., 2019b. URL <https://proceedings.neurips.cc/paper/2019/file/6775a0635c302542da2c32aa19d86be0-Paper.pdf>.
- Xiaoxiao Li, Yuan Zhou, Siyuan Gao, Nisha Dvornek, Muhan Zhang, Juntang Zhuang, Shi Gu, Dustin Scheinost, Lawrence Staib, Pamela Ventola, and James Duncan. Braingnn: Interpretable brain graph neural network for fmri analysis. *bioRxiv*, 2020. doi: 10.1101/2020.05.16.100057. URL <https://www.biorxiv.org/content/early/2020/05/17/2020.05.16.100057>.
- Yinhan Liu, Myle Ott, Naman Goyal, Jingfei Du, Mandar Joshi, Danqi Chen, Omer Levy, Mike Lewis, Luke Zettlemoyer, and Veselin Stoyanov. Roberta: A robustly optimized bert pretraining approach. *arXiv preprint arXiv:1907.11692*, 2019.
- Ilya Loshchilov and Frank Hutter. Decoupled weight decay regularization. *arXiv preprint arXiv:1711.05101*, 2017.
- Jiasen Lu, Dhruv Batra, Devi Parikh, and Stefan Lee. Vilbert: Pretraining task-agnostic visiolinguistic representations for vision-and-language tasks. In H. Wallach, H. Larochelle, A. Beygelzimer, F. d'Alché-Buc, E. Fox, and R. Garnett, editors, *Advances in Neural Information Processing Systems*, volume 32. Curran Associates, Inc., 2019. URL <https://proceedings.neurips.cc/paper/2019/file/c74d97b01eae257e44aa9d5bade97baf-Paper.pdf>.

- Andriy Myronenko. 3d mri brain tumor segmentation using autoencoder regularization. In *International MICCAI Brainlesion Workshop*, pages 311–320. Springer, 2018a.
- Andriy Myronenko. 3d mri brain tumor segmentation using autoencoder regularization. In *International MICCAI Brainlesion Workshop*, pages 311–320. Springer, 2018b.
- Atif Riaz, Muhammad Asad, SM Masudur Rahman Al-Arif, Eduardo Alonso, Danai Dima, Philip Corr, and Greg Slabaugh. Fcnet: a convolutional neural network for calculating functional connectivity from functional mri. In *International Workshop on Connectomics in Neuroimaging*, pages 70–78. Springer, 2017.
- Atif Riaz, Muhammad Asad, Eduardo Alonso, and Greg Slabaugh. Deepfmri: End-to-end deep learning for functional connectivity and classification of adhd using fmri. *Journal of neuroscience methods*, 335:108506, 2020.
- Karen Simonyan and Andrew Zisserman. Very deep convolutional networks for large-scale image recognition. *arXiv preprint arXiv:1409.1556*, 2014.
- Nitish Srivastava, Geoffrey Hinton, Alex Krizhevsky, Ilya Sutskever, and Ruslan Salakhutdinov. Dropout: a simple way to prevent neural networks from overfitting. *The journal of machine learning research*, 15(1):1929–1958, 2014.
- Martijn P. van den Heuvel and Hilleke E. Hulshoff Pol. Exploring the brain network: A review on resting-state fmri functional connectivity. *European Neuropsychopharmacology*, 20(8): 519–534, 2010. ISSN 0924-977X. doi: <https://doi.org/10.1016/j.euroneuro.2010.03.008>. URL <https://www.sciencedirect.com/science/article/pii/S0924977X10000684>.
- David C. Van Essen, Stephen M. Smith, Deanna M. Barch, Timothy E.J. Behrens, Essa Yacoub, and Kamil Ugurbil. The wu-minn human connectome project: An overview. *NeuroImage*, 80:62–79, 2013. ISSN 1053-8119. doi: <https://doi.org/10.1016/j.neuroimage.2013.05.041>. URL <https://www.sciencedirect.com/science/article/pii/S1053811913005351>. Mapping the Connectome.
- Ashish Vaswani, Noam Shazeer, Niki Parmar, Jakob Uszkoreit, Llion Jones, Aidan N. Gomez, Lukasz Kaiser, and Illia Polosukhin. Attention is all you need. In *Proceedings of the 31st International Conference on Neural Information Processing Systems, NIPS’17*, page 6000–6010, Red Hook, NY, USA, 2017a. Curran Associates Inc. ISBN 9781510860964.
- Ashish Vaswani, Noam Shazeer, Niki Parmar, Jakob Uszkoreit, Llion Jones, Aidan N Gomez, Lukasz Kaiser, and Illia Polosukhin. Attention is all you need. In *Advances in neural information processing systems*, pages 5998–6008, 2017b.
- N. D. Woodward and C. J. Cascio. Resting-State Functional Connectivity in Psychiatric Disorders. *JAMA Psychiatry*, 72(8):743–744, Aug 2015.
- Neo Wu, Bradley Green, Xue Ben, and Shawn O’Banion. Deep transformer models for time series forecasting: The influenza prevalence case, 2020.
- Yuxin Wu and Kaiming He. Group normalization. In *Proceedings of the European conference on computer vision (ECCV)*, pages 3–19, 2018.

- C. H. Xia, Z. Ma, R. Ciric, S. Gu, R. F. Betzel, A. N. Kaczkurkin, M. E. Calkins, P. A. Cook, A. García de la Garza, S. N. Vandekar, Z. Cui, T. M. Moore, D. R. Roalf, K. Ruparel, D. H. Wolf, C. Davatzikos, R. C. Gur, R. E. Gur, R. T. Shinohara, D. S. Bassett, and T. D. Satterthwaite. Linked dimensions of psychopathology and connectivity in functional brain networks. *Nat Commun*, 9(1):3003, 08 2018.
- Zhilin Yang, Zihang Dai, Yiming Yang, Jaime Carbonell, Russ R Salakhutdinov, and Quoc V Le. Xlnet: Generalized autoregressive pretraining for language understanding. *Advances in neural information processing systems*, 32, 2019.
- Bing Yu, Haoteng Yin, and Zhanxing Zhu. Spatio-temporal graph convolutional networks: A deep learning framework for traffic forecasting. *arXiv preprint arXiv:1709.04875*, 2017.
- X. Zhan and R. Yu. A Window into the Brain: Advances in Psychiatric fMRI. *Biomed Res Int*, 2015:542467, 2015.
- Liang Zou, Jiannan Zheng, et al. 3D CNN based automatic diagnosis of attention deficit hyperactivity disorder using functional and structural MRI. *IEEE Access*, 2017.

Supplementary Appendices⁷

6. More details about the HCP evaluations

The HCP dataset ([Van Essen et al., 2013](#)) originally incorporates 1200 subjects out of which 1096 are available at the ConnectomeDB website under the category - Resting State fMRI 1 Preprocessed. From the available 1096 subjects, we removed 1 subject which produced an error in the process of parcellation.

6.1. The HCP age labels

At the ConnectomeDB website, all subjects are listed with a respective metadata file, containing an age category (i.e. young/adult) and an associated ID number. The precise age used in our work was retrieved from the GitHub page of ([Gadgil et al., 2020](#)), which uploaded the data as a chart of subject IDs associated with accurate age.

6.2. HCP Gender Prediction Task

Tab. 6 depicts the performance of all models, evaluated on the gender prediction task. Here, we report the accuracy, balanced accuracy, AUC, precision, recall and f1 scores for each of the models.

6.3. HCP Age Prediction Task

Fig. 6 depicts three representative samples from the age prediction task. The figure presents the age predictions of all models for three subjects from the HCP test set, along with the ground truth and a representative slice from each of the scans.

⁷Put here for the reader’s convenience.

Model	Accuracy	BAC	AUC	Precision	Recall	F1
TFF	94.09	93.91	98.77	94.84	92.0	93.4
TFF _{no-pre-training}	92.06	93.18	95.34	93.56	92.0	92.77
ST-GCN	79.81	82.0	81.36	82.13	77.0	79.48
Deep-FMRI	65.45	66.91	78.0	58.45	83.0	68.59

Table 6: Gender prediction results on the HCP dataset.

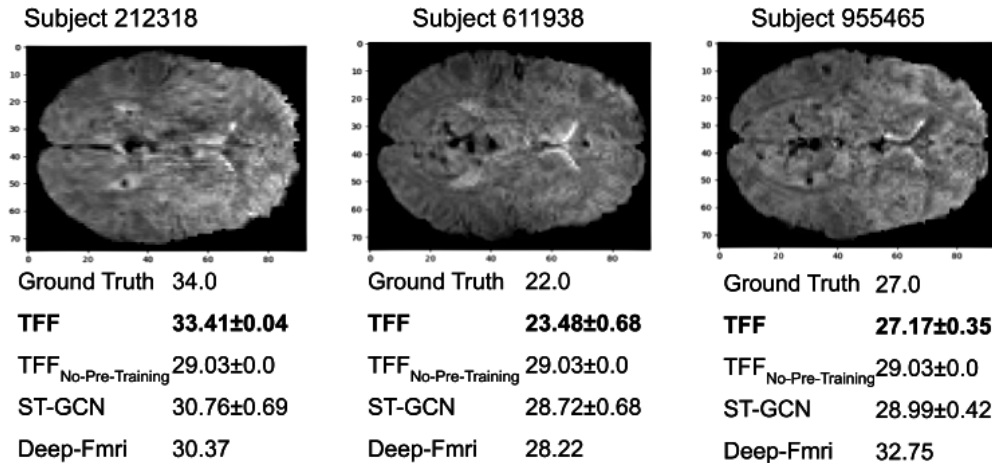


Figure 6: Three representative samples from the HCP test set, arbitrarily sliced at axial coordinate $z = 40$, together with the ground truth and predicted age retrieved by each model. For all models, except for the Deep-FMRI model, the average over sub-sequences is presented together with its corresponding standard deviation. Since Deep-FMRI operates on full scans, each subject corresponds to one sample and a single prediction..

7. The datasets splits

We randomly split each of the three datasets to train, validation, and test sets (70%-10%-20% respectively). The splits are attached as additional supplementary material (see `dataset_splits.zip`).

8. More details about the baselines

In both the Deep-fMRI and ST-GCN baselines, we kept all hyperparameters suggested by the authors. An early stopping protocol was enforced with a patient of 30 epochs, entailing that the training stopped only if 30 epochs have passed without any improvement on the validation set.

For both baselines, we performed a grid search over two parameters: the learning rate and the window size w . As suggested in the original ST-GCN work, given an fMRI scan, we

name	operations	repeats	output size
Input	Batch of fMRI volumes. Global and voxel norm aggregated on the channel dim	1	(2x75x93x81)
Conv Block 1	Conv, Dropout	1	(4x75x93x81)
Regular Block 1	GroupNorm, LReLU, Conv, GroupNorm, LReLU, Conv	1	(4x75x93x81)
Down Block 1	Dropout, Conv (stride 2)	1	(5x8x38x47x41)
Regular Block 2	GroupNorm, LReLU, Conv, GroupNorm, LReLU, Conv	2	(5x8x38x47x41)
Down Block 2	Dropout, Conv (stride 2)	1	(5x16x19x24x21)
Regular Block 3	GroupNorm, LReLU, Conv, GroupNorm, LReLU, Conv	2	(5x16x19x24x21)
Down Block 3	Dropout, Conv (stride 2)	1	(5x32x10x12x11)
Regular Block 4	GroupNorm, LReLU, Conv, GroupNorm, LReLU, Conv	4	(5x32x10x12x11)
Reduce Block	GroupNorm, LReLU, Conv	1	(5x2x10x12x11)
Flatten	Flatten	1	(5x2640)

Table 7: The architecture of the 3D encoder network \mathcal{E} . Unless mentioned otherwise, all Convolution operations utilize a kernel of size 3, stride 1, and padding 1.

name	operations	repeats	output size
Input	output of the encoder / attention output sequences aggregated on batch dim	1	(5x2640)
Linear Block	Linear	1	(5x2640)
Expand Dim	UnFlatten, GroupNorm, LReLU, Conv	1	(5x32x10x12x11)
Up Block 1	Conv (kernel size 1), UpSample	1	(5x16x19x24x21)
Regular Block 1	GroupNorm, LReLU, Conv, GroupNorm, LReLU, Conv	1	(5x16x19x24x21)
Up Block 2	Conv (kernel size 1), UpSample	1	(5x8x38x47x41)
Regular Block 1	GroupNorm, LReLU, Conv3d, GroupNorm, LReLU, Conv	1	(5x8x38x47x41)
Up Block 3	Conv (kernel size 1), UpSample	1	(5x4x75x93x81)
Regular Block 1	GroupNorm, LReLU, Conv, GroupNorm, LReLU, Conv	1	(5x4x75x93x81)
Final Block	Conv, Conv (kernel size 1)	1	(5x1x75x93x81)

Table 8: The architecture of 3D the decoder network \mathcal{D} .

randomly sampled sub-sequences of size w from the full scan and propagated the sub-sequence through the network.

9. More details about the TFF architecture

The TFF architecture consists of three components: (i) 3D Convolutional encoder, (ii) transformer, and (iii) 3D Convolutional decoder. Tab. 7 and Tab. 8 present the detailed architecture of the 3D encoder and decoder networks, respectively.

The implementation of the transformer architecture is based on the hugging face library⁸. Our code is attached as an additional supplementary.

During the first pre-training step, only the 3D encoder and the decoder are trained. In the second step, the transformer is integrated between the encoder and the decoder, and the entire architecture is trained to optimize the pre-training objective.

During fine-tuning, we remove the decoder, and only the encoder-transformer networks are trained, where the transformer operates on an additional CLS token that is concatenated to the beginning of each sequence. The CLS embedding is then propagated through an MLP to score a regression/classification objective.

⁸https://huggingface.co/transformers/_modules/transformers/models/bert/modeling_bert.html#BertModel